JOURNAL OF MAGNETIC RESONANCE **129,** 44–52 (1997)
ARTICLE NO. MN971243

^{2}H Double-Quantum NMR Spectroscopy for the Study of Molecular Motion in Solids

Melinda J. Duer and Clare Stourton

Department of Chemistry, University of Cambridge, Lensfield Road, Cambridge CB2 1EW, Great Britain

Received January 14, 1997; revised July 30, 1997

An experiment which separates ^{2}H spinning sideband patterns according to the ^{2}H double-quantum chemical shift in a manner suitable for motional studies is proposed. The technique is successfully applied to 4,4′-azoxydianisole at 323 K to separately analyze the motion of the aromatic and methyl deuterons. Comments are made on the formation of a nematic mesophase in this material at 390 K in the light of the results of this NMR study. © 1997 Academic Press

I. INTRODUCTION

^{2}H NMR spectra have and continue to be one of the most important tools available for the study of molecular dynamics in solids (*1–3*). This spin-1 nucleus suffers a relatively small quadrupole coupling (on the scale of quadrupole coupling magnitudes in general) which broadens the corresponding NMR lines to first order in the quadrupole coupling. In turn, the strength of the quadrupole coupling interaction is dependent upon molecular orientation, so that changes in molecular orientation manifest themselves as distortions of the NMR lineshape caused by averaging of the resonance frequencies which appear during the course of the motion. Both broadline (*1–3*) and magic-angle spinning (MAS) exchange (*4*) spectra have been used in motional studies. The shortcomings of broadline spectroscopy are self-evident: lines from different chemical sites overlap, and the consequent loss of resolution prohibits analysis of the lineshapes for motional studies. Magic-angle spinning goes part way to alleviating this problem by reducing the broadline spectrum to a series of sharp lines, one at the isotropic chemical shift, and a set of spinning sidebands spaced by the sample spinning speed, providing that the spinning speed is less than the width of the quadrupolar-broadened line. The hope would be that the spinning sideband patterns from different chemical sites can be resolved, and then each separately analyzed to reveal motional details. However, the chemical shift range for ^{2}H in organic solids, for instance, is small, and often, similar sites cannot be resolved by MAS as the line broadening still inherent in the spectra is of similar magnitude to the chemical shift differences between inequivalent sites.

In this work we propose a practicable solution to this problem of resolution in ^{2}H NMR spectroscopy which still allows measurement of a spectrum from which motional details can be deduced. We propose an experiment which uses double-quantum (DQ) chemical shifts to separate ^{2}H MAS spinning sideband patterns (or alternatively, broadline spectra) in a two-dimensional experiment. DQ NMR spectroscopy for ^{2}H has been proposed in the past. Pioneering work by Pines and Vega (*5–7*) drew attention to its potential 20 years ago. However, it has never been taken up or developed by other spectroscopists. One of the reasons may have been that this early work was justifiably primarily interested in the double-quantum spectrum itself. Other than improved resolution, this spectrum gives no extra information above the normal single-quantum spectrum. In addition, the work of Pines and Vega (*5, 6*) makes clear that the amplitude of double-quantum coherence excited in their experiment depends on the strength of quadrupole coupling and hence upon molecular orientation. Thus, it is not clear that spinning sideband patterns (or broadline powder patterns) subsequently produced from that DQ coherence will contain information about sufficient molecular orientations for the spectra to be useful in motional studies.

In this work we demonstrate that it is possible to excite DQ coherence sufficiently evenly across different molecular orientations and different molecular sites in general that sensible motional studies can be undertaken. We consider how the spinning sideband patterns arising from the DQ experiment can be analyzed quantitatively to reveal details about the particular molecular motions present in a sample.

Finally, the method is applied to fully deuterated 4,4′-azoxydianisole, where the resolution afforded in the DQ spectrum allows the separate analyses of the motion of the methyl and aromatic deuterons. 4,4′-Azoxydianisole forms a nematic phase at 390 K (*8*) and the analysis of molecular motion in the solid state sheds some light on the formation of this phase.

II. EXPERIMENTAL

All spectra were recorded on a Chemagnetics CMX 400 spectrometer operating at 61.4 MHz for ^{2}H. The spinning

1090-7807/97 $25.00

TABLE 1
The Phase Cycling Used in the DQ-Filtered Experiment with the Pulse Sequence $90°-\tau-90°-t_1-90°-t_2$

Pulse 1/degrees	Pulse 2/degrees	Receiver/degrees
0	0	0
90	90	180
180	180	0
270	270	180
180	0	180
270	90	0
0	180	180
90	270	0

speed was controlled to within ±5 Hz of the recorded value by standard Chemagnetics equipment.

The sample of fully deuterated 4,4′-azoxydianisole (Aldrich) was used without further purification. The DQ-filtered experiment with $90^\circ_x-\tau-90^\circ_x$ excitation of the DQ coherence was used to record two two-dimensional datasets, in which the two 90° excitation pulses differed in phase by 45° between the two cases. The phase cycling used is given in Table 1 and includes cycling the two 90° excitation pulses in steps of 180° while keeping the receiver phase constant to select ±2 quantum coherence in t_1. The final pulse was not cycled. The 90° pulse length was 3.4 μs and a 15-s delay between scans was employed. The τ delay was 10 μs, the dead time was 14 μs, and the sample spinning speed was 10 kHz. The t_1 delay was synchronized with the rotor period, giving an f_1 spectral width of 10 kHz; 3072 t_2 points were collected for each of 80 t_1 points.

The two datasets were processed in the hypercomplex manner using the method of Spiess and co-workers (*9*). One hundred hertz Gaussian line broadening was employed in t_1, and 50 Hz in t_2. This produces a DQ spectrum in f_1 which is correlated with spinning sideband patterns in f_2. Broadline spectra in f_2 could be produced by Fourier transformation of just a half of one rotational echo in the t_2 dataset, rather than the whole FID.

III. THEORY

In order to assess the efficiency of the DQ-filtered experiment it is necessary to calculate the FID resulting from different experimental conditions. This is done by calculating the density matrix ρ within the Zeeman basis at the end of the applied pulse sequence, and then following the time evolution of desired n-quantum terms of ρ (i.e., ρ^{i-j}, where $j-i=n$) to form an ''FID'' of the n-quantum coherence.

To calculate the density operator at any point in time the equation (*10*)

$$\rho(\tau) = \mathbf{U}(\tau)\,\rho(0)\,\mathbf{U}^{+}(\tau), \qquad [1]$$

where the propagator matrix $\mathbf{U}(\tau)$ is

$$\mathbf{U}(\tau) = \hat{T}\exp\left(-i\int_0^\tau \mathbf{H}(t)\,dt\right), \qquad [2]$$

must be evaluated, by integrating Eq. [2] numerically (*11*) with the relevant Hamiltonian matrix, $\mathbf{H}(t)$, being employed for time periods where RF pulses are applied and time periods of free precession. The Hamiltonian operator in the rotating frame to first order under MAS which is employed during periods of free precession is H_{fp},

$$\begin{aligned} H_{\mathrm{fp}} &= H_{\mathrm{Z}} + H_{\mathrm{Q}}^{(1)} \\ &= -\Delta\omega T_{10} + \frac{eQ}{4I(2I-1)h}\sqrt{6}\,V_{20}T_{20}, \end{aligned} \qquad [3]$$

where the first term is the Zeeman term and the second is due to the first-order quadrupole coupling. The T_{k0} terms are tensor operators:

$$\begin{aligned} T_{10} &= I_z \\ T_{20} &= \sqrt{\frac{1}{6}}\left(3I_z^2 - I(I+1)\right). \end{aligned} \qquad [4]$$

The V_{20} term arises from the quadrupole coupling tensor. It can be expressed in terms of Wigner rotation matrices which relate the principal axis frame (PAF) of the quadrupole tensor to a frame attached to the sample rotor and those which relate the rotor frame to the laboratory frame (*12*),

$$V_{20} = \sum_m D_{m0}^{(2)}(\omega_{\mathrm{R}}t, \theta_{\mathrm{R}}, 0)\sum_n D_{nm}^{(2)}(\alpha, \beta, \gamma)\,A_{2n}, \qquad [5]$$

with

$$A_{20} = \frac{1}{14}(\eta^2 - 3), \quad A_{2\pm2} = \frac{1}{7}\sqrt{\frac{3}{2}}\eta. \qquad [6]$$

The Hamiltonian operator during an RF pulse (also in the rotating frame) is H_{p}:

$$\begin{aligned} H_{\mathrm{p}} &= H_{\mathrm{fp}} + H_{\mathrm{RF}} \\ &= H_{\mathrm{fp}} + \frac{\omega_1}{\sqrt{2}}\left(T_{1-1}\exp(+i\phi) - T_{11}\exp(-i\phi)\right). \end{aligned} \qquad [7]$$

ω_1 is the amplitude of the RF pulse and ϕ its phase. The tensor operators are defined as

$$T_{1\pm1} = \mp\sqrt{\frac{1}{2}}\,I_{\pm}. \qquad [8]$$

The initial density operator $\rho(0)$ in Eq. [1] at the start of the pulse sequence is simply that for the spin system at equilibrium

$$\rho(0) = \left(\frac{\hbar\omega_L}{kT}\right) I_z, \qquad [9]$$

where ω_L is the Larmor frequency.

A complete NMR lineshape is produced by sampling the n-quantum terms of the density matrix at time intervals of (spectral width)$^{-1}$ as it evolves under the Zeeman and quadrupole Hamiltonians (Eq. [3]). The resulting FID for different molecular orientations, representing those of a powder sample, are summed, and the resultant Fourier transformed to produce a frequency spectrum.

Typically, the numerical integration uses 100 points per rotor period and FIDs from 256,000 different molecular orientations are summed to produce a powder spectrum.

IV. EXCITATION OF DQ COHERENCE

The quadrupole coupling for ^{2}H spins in most environments is relatively small compared with the Zeeman coupling. Thus, to excite DQ coherence in ^{2}H it is possible to use the $90°-\tau-90°$ pulse sequence which is used to excite multiple-quantum coherences in solution NMR (*10*). Single pulses have also been used to excite multiple-quantum coherences (*5, 13*) for spin -1 and spin >1, and so we investigate their use under magic-angle spinning as well. Figure 1 shows how the DQ coherence excitation by a single pulse varies with pulse length for different pulse amplitudes, ω_1. Clearly, there are several optimal pulse amplitude/pulse length combinations which generate sufficient DQ coherence for use in the intended experiment.

However, the problem encountered in multiple-quantum methods for quadrupolar nuclei in solids is generally that the efficiency of generating a multiple-quantum coherence

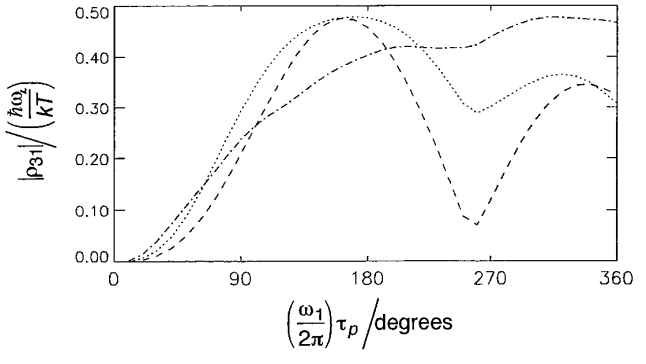

FIG. 1. The variation of magnitude of DQ coherence excited by a single pulse of varying length for three different pulse amplitudes ω_1. The amplitude of DQ coherence plotted is the total arising (from all molecular orientations) for a powder sample. ·−·−·, ω_1 = 20 kHz; · · ·, ω_1 = 50 kHz; - - -, ω_1 = 100 kHz.

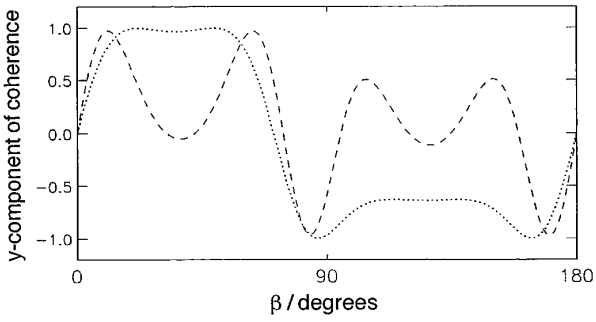

FIG. 2. (Dashed line) Angular dependence of double-quantum excitation profile for the $90^\circ_x-\tau-90^\circ_x$ excitation sequence. (Dotted line) Angular dependence of double-quantum excitation profile for single-pulse excitation. The y component of the double-quantum coherence $(1/2i)(\rho_{13} - \rho_{31})/(\hbar\omega_L kT)$, where ω_L is the Larmor frequency, is plotted against β, where β is the angle between the sample spinning axis and the unique axis of the ^{2}H quadrupole tensor. Both calculations assume quadrupole parameters e^2qQ = 180 kHz, asymmetry, $\eta = 0$, other orientation angles, $\alpha = 0°$ and $\gamma = 0°$, and sample spinning speed 10 kHz. For the $90^\circ_x-\tau-90^\circ_x$ excitation, $\tau = 5$ μs and 90° pulse length = 3 μs. For single-pulse excitation, the pulse amplitude $\omega_1/2\pi$ = 50 kHz and pulse length $(\omega_1/2\pi)\tau_p = 160°$.

varies markedly with the quadrupole splitting (*5, 6, 13*), i.e., with the molecular orientation in a powder sample, or with chemical site in general. If the DQ method is to be used to study molecular motion which consists of changes in molecular orientation, it is important that all molecular orientations are excited and preferably relatively evenly. Thus, we have investigated how far this is the case for both possible excitation methods, and how the experiment responds to changes in the experimental variables.

Figure 2 compares the size of the y component of the DQ coherence arising from a $90°-\tau-90°$ excitation sequence and a single pulse, for different molecular orientations with respect to the sample spinning axis for a spinning rate of 10 kHz. The single pulse chosen ($(\omega_1/2\pi)\tau_p = 160°$ and ω_1 = 50 kHz) is one shown to be optimal by the calculations illustrated in Fig. 1. For the $90°-\tau-90°$ sequence, hard 90° pulses are required, so the calculations are performed with a 90° pulse length of 3 μs, which corresponds to a pulse power most spectrometers are capcable of. Clearly, there is variation in the amount of the DQ coherence excited with molecular orientation for both methods of excitation, slightly more so for the $90°-\tau-90°$ excitation. However, for neither method of excitation are there many null points, where no DQ coherence is excited. On this result, we may hope that the ^{2}H spinning sideband patterns arising in the DQ-filtered experiment using either excitation method contain significant information from sufficient molecular orientations that they may be usefully used in motional studies.

Figure 3 shows how the f_2 single-quantum spectra resulting from DQ experiments using single-pulse excitation compare with that from a simple 90° pulse–acquire experiment. Figure 4 shows the f_2 single-quantum spectra which result when a $90°-\tau-90°$ excitation sequence is used, and

illustrates the effect of varying the τ delay. These spectra too are to be compared with the ''ideal'' single-quantum spectrum arising from a simple 90° pulse–acquire experiment in Fig. 3. Those spectra resulting from the DQ experiment employing a $90°-\tau-90°$ excitation and low τ times compare most favorably both in terms of overall intensity and in terms of spinning sideband pattern with that from the 90° pulse–acquire experiment. Exact correspondence here is not necessary as any simulations of experimental spectra will in any case be performed assuming the complete DQ pulse sequence and the experimental parameters. However, it would be a cause for concern if the f_2 spectra resulting from the DQ experiment showed significantly narrower spinning sideband patterns, for instance, or patterns with very different intensity distributions to the single-pulse spectrum, indicating that many molecular orientations were not represented in the spectra. It is worth noting, however, that there will be no DQ intensity to first order for the $90°-\tau-90°$ excitation method when $\tau = \tau_R$, the rotor period, as in that case, the

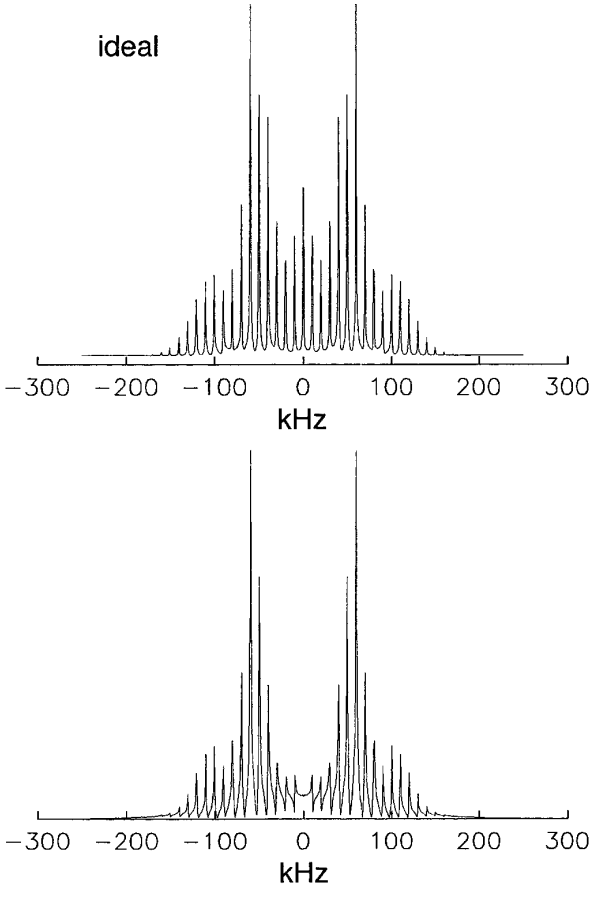

FIG. 3. Comparing ^{2}H spinning sideband patterns calculated to arise from a simple 90° (3 μs) pulse–acquire experiment (top) and the double-quantum-resolved experiment using single-pulse excitation of the DQ coherence (bottom). For the latter spectrum, the single pulse assumed is the same as that for Fig. 2 and with 1000 f_2 points calculated for $t_1 = 0$. The sample spinning speed for both spectra is 10 kHz.

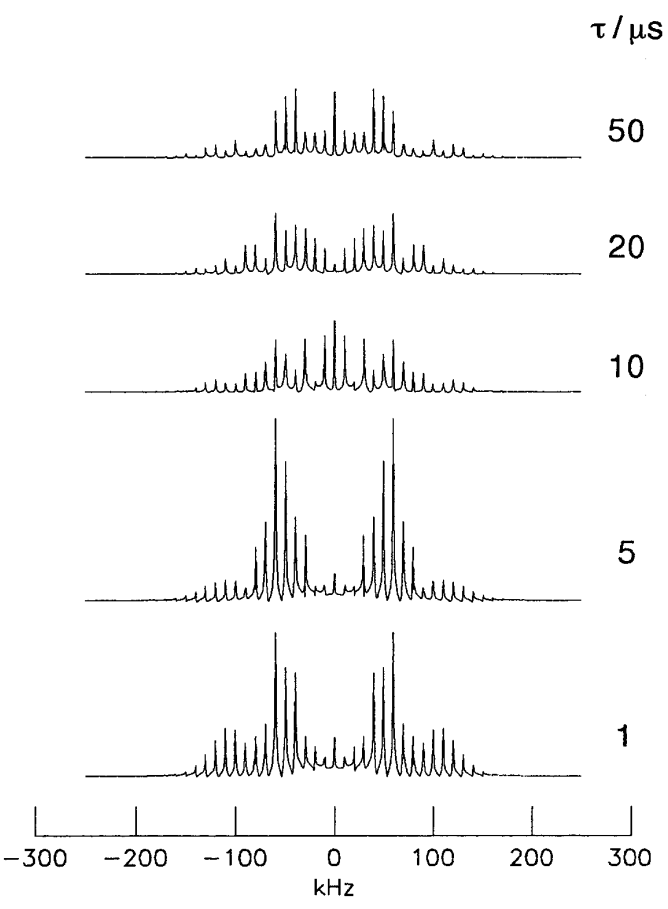

FIG. 4. Calculated f_2 spinning sideband patterns arising from the $90^\circ_x-\tau-90^\circ_x-\tau_1-90^\circ_x-t_2$ double-quantum-filtered pulse sequence for different values of τ. The calculations assume quadrupole parameters e^2qQ = 180 kHz, asymmetry, $\eta = 0$, sample spinning speed 10 kHz, and 90° pulse length = 3 μs with 1000 f_2 points calculated for $t_1 = 0$.

average quadrupole splitting over the τ period is zero for all molecular orientations. With this proviso, Figs. 3 and 4 show no clear advantage to either excitation method, but suggest that both methods are feasible.

Figure 5 investigates how the overall magnitude intensity of the f_2 spectra arising from experiments using the $90°-\tau-90°$ excitation is affected by the sample spinning speed. While there are variations in intensity with spinning speed, these are not order of magnitude variations, and we can conclude that the particular spinning speed chosen for an experiment is not critical, providing of course that $\tau \neq \tau_R$.

V. MOLECULAR MOTION

Here, we consider the effects of molecular motions upon the MAS single-quantum (SQ) spectra in the f_2 dimension of the two-dimensional spectrum. It is expected that the spinning sideband patterns resolved in this dimension according to their DQ chemical shift will be good monitors of molecular motion as discussed in the previous section, in the

same way that one-dimensional spectra of simpler chemical systems are used. We have found that computations of the f_2 spectra for the DQ experiment using single-pulse excitation of the DQ coherence are prohibitively long, since we must take into account molecular motion during the relatively long excitation pulse. Thus, it is probably not realistic to attempt to ''fit'' DQ ^{2}H obtained by this excitation method, as such fitting can be generally expected to involve many trial calculations. Accordingly, we henceforth consider only the $90°-\tau-90°$ method of exciting DQ coherence.

We consider rotational motions only, i.e., those in which the resonance frequency of a particular nuclear site changes by virtue of a change in orientation of the corresponding quadrupole tensor, not due to chemical exchange between inequivalent sites. We assume that the rotations occur by Markovian exchange between N discrete sites. Since we want to calculate the f_2 MAS spectrum integrated over the DQ lineshape, the f_2 spectrum is calculated for $t_1 = 0$ for each inequivalent site for the DQ-filtered pulse sequence discussed in Section IV. We also assume perfect, nonselective 90° pulses, which are sufficiently short that effectively no molecular motion occurs during them. Molecular motion may occur during any periods of free precession. Since we are interested only in the case where $t_1 = 0$, the only period of free precession up to the start of t_2 in the DQ pulse sequence is the τ delay during the DQ excitation sequence.

The complete DQ pulse sequence is analyzed in Fig. 6 for a nonspinning sample in terms of Cartesian spin operators. When the sample is spinning, the quadrupole splitting frequency, ω, is of course time-dependent, but this does not alter the basic conclusions of the analysis. The density operator evolves during the τ delay under first-order quadrupole coupling into an oscillating linear combination of I_y and D_{xz} terms. DQ coherence in t_1 is then produced by the action of the second $90°_x$ pulse on the D_{xz} term in the density operator. Finally, the DQ coherence is transformed into observable single-quantum coherence in t_2 by the action of a third 90° pulse. Specifically, in t_2, the spin system is again described by a density operator consisting of an oscillating linear combination of I_y and D_{xz} terms, the I_y component of which gives rise to the observable signal. The evolution of the density operator in t_2 can be expressed most usefully by constructing a complex function $\rho^+(t)$ which describes the components of the density operator,

$$\text{Re}\left(\rho^+(t_2)\right) = A_{xz}(t_2)$$
$$\text{Im}\left(\rho^+(t_2)\right) = A_y(t_2), \qquad [10]$$

where $A_{xz}(t_2)$ and $A_y(t_2)$ are the amplitudes of the D_{xz} and I_y components of the density operator, respectively. Then the time dependence of ρ^+ can be expressed as

$$\frac{d\rho^+(t_2)}{dt_2} = i\omega(t_2)\rho^+(t_2), \qquad [11]$$

where ω is the quadrupole frequency of the spin due to its particular orientation. Note that the time dependence of ω induced by magic-angle spinning has been included. In an N-site system, $\rho^+(t_2)$ becomes an N-dimensional vector, $\boldsymbol{\rho}^+(t_2)$, with one component describing the density operator associated with each site. Exchange between the N sites is mediated through an $N \times N$ kinetic matrix $\mathbf{W}$, where an

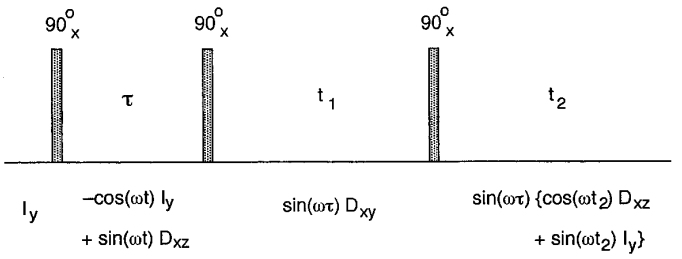

FIG. 6. The double-quantum-filtered pulse sequence (top) and the corresponding density operator (below) for an isolated spin-1 system under first-order quadrupole coupling. The analysis is for a static sample, i.e., nonspinning, and the density operator is expressed in terms of Cartesian tensor coordinates. ω is the quadrupole frequency of the spin, which is dependent upon the orientation of the quadrupole principal axis frame in the applied magnetic field. Only double-quantum terms are assumed to survive in t_1 (arranged experimentally by phase cycling). Note that the $\sin(\omega\tau)$ factor introduced during the τ delay (the amplitude of the D_{xz} term in the density operator at the end of the τ period) is a constant factor throughout the remainder of the pulse sequence.

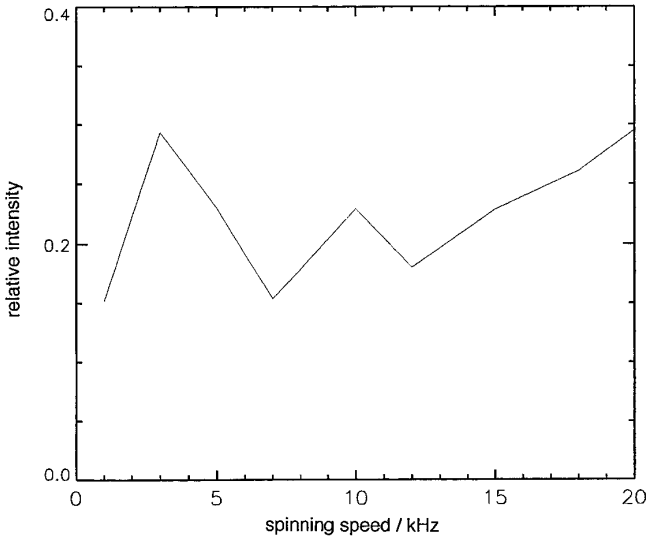

FIG. 5. Calculated magnitude intensity of DQ-filtered f_2 spectra as a function of sample spinning speed. The magnitudes are expressed relative to the magnitude intensity of the spinning sideband pattern resulting from a simple 90° pulse–acquire experiment conducted at a spinning rate of 10 kHz. All calculations assume quadrupole parameters $e^2qQ = 180$ kHz, asymmetry, $\eta = 0$, 90° pulse length = 3 μs, and for the DQ experiment, $\tau = 5$ μs with 1000 f_2 points calculated for $t_1 = 0$.

element W_{jk} is given by the jump rate from site k to j. The differential equation describing the time dependence of $\boldsymbol{\rho}^+(t_2)$ is then given by (*1, 14*)

$$\frac{d\boldsymbol{\rho}^+(t_2)}{dt_2} = \{i\Omega(t_2) + \mathbf{W}\}\rho^+(t_2), \qquad [12]$$

where $\Omega(t_2)$ is an $N \times N$-dimensional diagonal matrix, with elements $\omega_j(t)$ which are the quadrupole frequency of the $j$the site.

In the absence of MAS, Ω is time-independent, and Eq. [12] can be integrated directly to yield

$$\boldsymbol{\rho}^+(t_2) = \mathbf{L}(t_2)\boldsymbol{\rho}^+(0), \qquad [13]$$

where $\rho^+(0) = A_{xz}(0)$, since $A_y(0) = 0$ (see Fig. 6) and

$$\mathbf{L}(t_2) = \exp\{(i\Omega + \mathbf{W})t_2\}. \qquad [14]$$

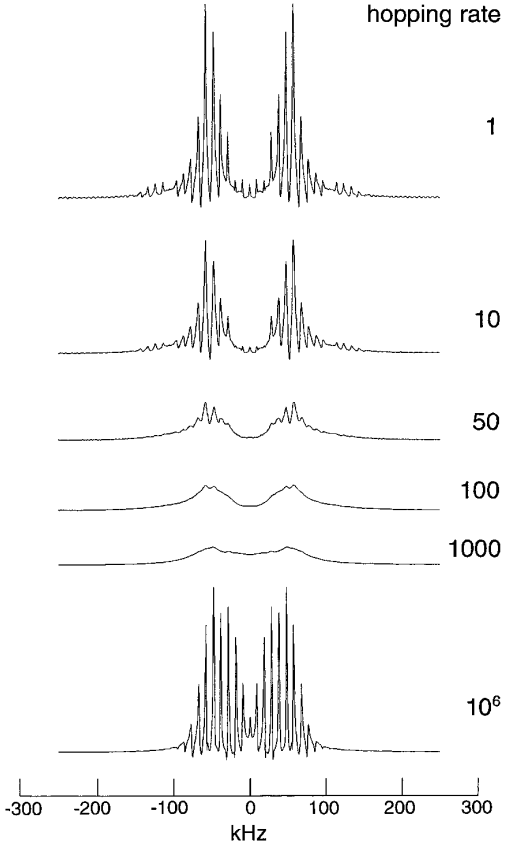

FIG. 7. Illustration of the effects of molecular motion on the ^{2}H spinning sideband patterns arising from the DQ-filtered pulse sequence. The spectra are calculated assuming that the deuteron hops between two sites in which orientation of the unique axis of the (axial) ^{2}H quadrupole tensor differs by 120°. Spectra are calculated for different rates of motion as detailed in the figure. The calculation uses quadrupole parameters $e^2qQ = 180$ kHz, asymmetry, $\eta = 0$, and $\tau = 5$ μs. The details of the calculation are discussed in the text.

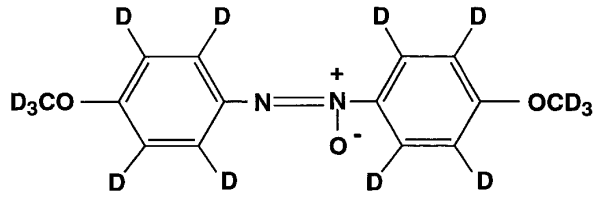

FIG. 8. Molecular structure of 4,4′-azoxydianisole.

This can be solved by diagonalizing $(i\Omega + \mathbf{W})$ (*14*). In the presence of MAS, the solution has the same form as Eq. [13], but now the propagator $\mathbf{L}(t_2)$ must be calculated iteratively (*11*), as the superoperator $(i\Omega(t_2) + \mathbf{W})$ does not commute with itself at different times t_2. In these circumstances, $\mathbf{L}$ can be estimated by dividing the rotor period up into n equal periods, Δt; then at the equally spaced time points, t_m, $\mathbf{L}$ is found through the iterative scheme

$$\mathbf{L}(m\Delta t) = \exp\{(i\Omega(t_m) + \mathbf{W})\Delta t\} \times \mathbf{L}(m-1)\Delta t)$$
$$\mathbf{L}(0) = \mathbf{1}. \qquad [15]$$

The FID signal, $s_+(t_2)$, in t_2 arising from each transition is derived from Eq. [13]:

$$s_+(t_2) = \mathrm{Im}\{\mathbf{1}\cdot\mathbf{L}(t_2)\cdot\boldsymbol{\rho}^+(0)\}. \qquad [16]$$

This signal can be calculated if we know $\boldsymbol{\rho}^+(0)$, the amplitudes of the D_{xz} components of the density operators associated with each of the N sites at $t_2 = 0$. The D_{xz} component of the density operator in t_2 arises directly from the DQ coherence in t_1 (Fig. 6) which in turn arises from the D_{xz} component in the density operator at the end of the τ delay. Thus, the amplitude of the D_{xz} component in the density operator at the start of t_2 is equal (for $t_1 = 0$, the only case we are interested in) to the amplitude of the D_{xz} component at the end of the τ delay, assuming perfect, hard 90° pulses perform the intervening transformations of coherence.

The amplitudes of the D_{xz} components at the end of τ are readily calculated taking into account magic-angle spinning and exchange in a similar calculation to that detailed above. We construct a complex function $\rho^+(t)$ as for $\rho^+(t_2)$ in Eq. [10] where the real and imaginary parts describe the amplitudes of the D_{xz} and I_y components respectively of the density operator which acts during τ for a single site. The time dependence of $\boldsymbol{\rho}^+(t)$ for an N-site exchanging system is then described by Eq. [12] (with t_2 replaced by t), which in turn can be solved numerically using Eqs. [13] and [15]. $\boldsymbol{\rho}^+(t = 0)$ is simply $-i$ in this case, as the density operator at the start of the τ delay is $-I_y$. The desired amplitudes of the D_{xz} components of the density operators for each of the N sites at the end of τ are then simply the real parts of $\boldsymbol{\rho}^+(\tau)$.

Subsequent Fourier transformation of the FID in Eq. [16]

yields a frequency spectrum which consists of a spinning sideband pattern whose linewidths and intensity distribution depend upon the nature of the molecular motion and its rate relative to the quadrupole coupling constant and spinning speed.

Figure 7 shows simulations of f_2 spectra for a two-site motion where the principal axis of the (axial) quadrupole tensor hops through 120° for increasing hopping speeds. It is to be noted that the ^{2}H spectrum exhibits characteristic line broadening and diminished intensity when the hopping rate is of similar magnitude to e^2qQ.

VI. RESULTS AND DISCUSSION

The DQ experiment using $90°-\tau-90°$ excitation of DQ coherence was performed on a solid sample of fully deuterated 4,4′-azoxydianisole (Fig. 8) at 323 K. The conventional one-dimensional, single-quantum ^{2}H MAS NMR spectrum is shown in Fig. 9. The isotropic shifts corresponding to the aromatic and methyl deuterons are not completely resolved, and resolution of the spinning sideband patterns is less good still. In particular, the low-intensity, higher-order spinning sidebands associated with the methyl resonance are swamped by the aromatic signals which are close to maximum intensity in this region. The f_1 DQ spectrum is shown in Fig. 10. This shows two well-resolved signals at −6.4 and +1.1 ppm relative to liquid C_6D_6 at 0 ppm corresponding to the methyl and aromatic deuterons, respectively. The latter peak is asymmetric in shape, presumably due to the presence of two incompletely resolved signals from the two different types of aromatic deuteron. The baseline wiggles are due to truncation of the t_1 FID. In solution, the ^{1}H resonances of 4,4′-azoxydianisole occur at 3.85, 6.95, and 8.25 ppm, respectively, thus giving an average methyl–aromatic signal separation of 3.8 ppm which agrees well with the solid-state DQ methyl–aromatic signal separation of 7.5 ppm.

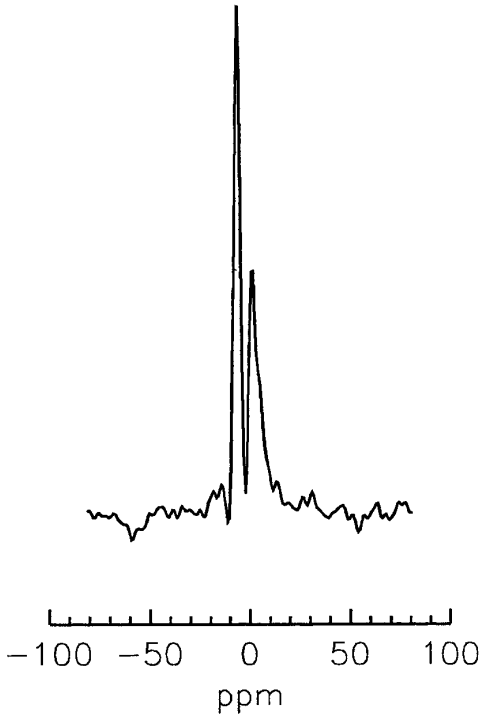

FIG. 10. The double-quantum ^{2}H spectrum for fully deuterated 4,4′-azoxydianisole. The two signals correspond to the methyl (−6.4 ppm) and the aromatic (+1.1 ppm) deuterons. Frequency is relative to the ^{2}H resonance of C_6D_6 at 0 ppm.

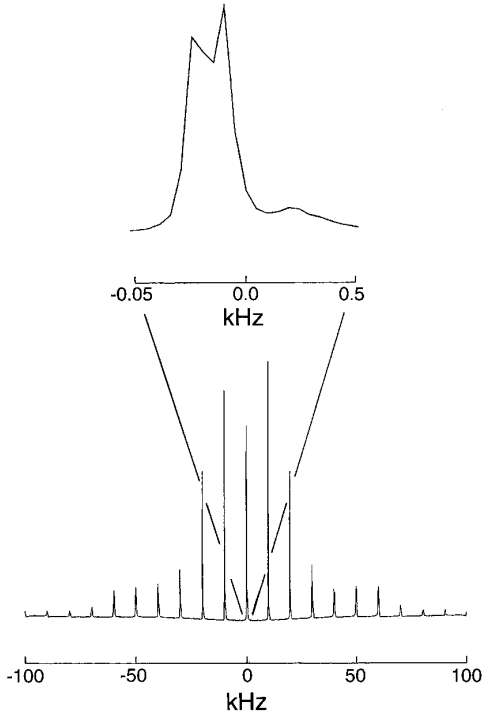

FIG. 9. The one-dimensional ^{2}H MAS NMR spectrum of 4,4′-azoxydianisole for a spinning speed of 10 kHz. The inset at the top of the figure shows an expansion of the centerband region.

Slices through the DQ signals in the f_2 dimension reveal the spectra shown in Fig. 11. The spinning sideband pattern for the methyl resonance is characteristically narrow, indicating that the CD_3 group is rotating rapidly around the C—O bond and indeed the simulated spectrum for such a motion (also Fig. 11) agrees well with the experimental one.

The f_2 spectra for the aromatic deuterons can be simulated by assuming static phenyl rings. The two different aromatic signals are not completely resolved, and so the experimental f_2 spectra here are the superposition of two independent spinning sideband patterns, corresponding to potentially different quadrupole coupling constants. The simulation in Fig. 11 represents the best fit when assuming that both sites have the same quadrupole coupling parameters (e^2qQ = 190 kHz; $\eta = 0$).

Molecular motion in the solid state has important conse-

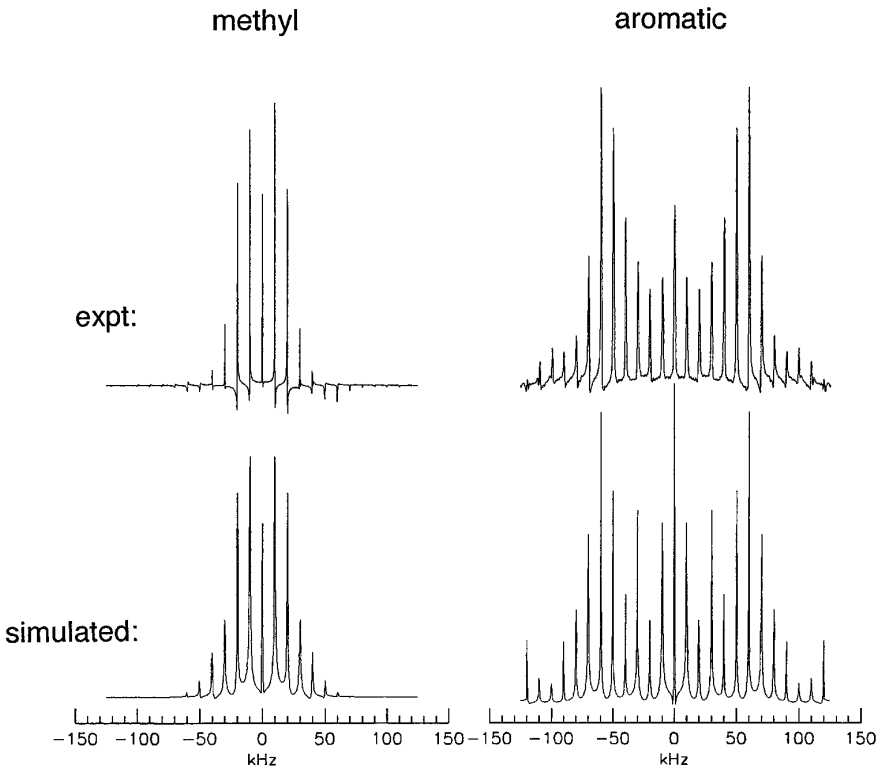

FIG. 11. The f_2 DQ-resolved spinning sideband spectra for the methyl and aromatic deuterons of fully deuterated 4,4′-azoxydianisole. Experimental spectra are sums of the f_2 slices from the two-dimensional spectrum over the width of the respective DQ (f_1) signal. The simulated spectra are calculated using the method in Section III. The quadrupole parameters for the methyl deuteron simulation are $e^2qQ = 57$ kHz and $\eta = 0$, which are the effective quadrupole parameters expected for a rapidly ($\gg e^2qQ$) spinning methyl group. The quadrupole parameters for the aromatic simulations are $e^2qQ = 190$ kHz and $\eta = 0$; both aromatic deuteron sites are assumed to have the same quadrupole parameters.

quences for the stability of any mesophase at higher temperatures. The temperature of a phase change is given by

$$T_{pc} = \frac{\Delta H_{pc}}{\Delta S_{pc}}, \qquad [17]$$

where ΔH_{pc} is the enthalpy, and ΔS_{pc} the entropy of the phase transition. A stable mesophase is formed only if the mesophase has a well-defined and nonzero temperature range for its existence. If the temperature of the solid–liquid-crystalline (LC) transition is too similar to that for the LC–isotropic liquid transition, then the solid tends to melt directly to an isotropic liquid. In order to avoid this situation, ΔS for the solid–LC transition needs to be large relative to that for the LC–isotropic transition. ΔS in turn is related to the difference in the degree of disorder between the two phases. In many compounds containing *para*-substituted phenyl rings, the rings are found to undergo librational motions of increasing amplitude and/or rate as the temperature is increased, with 180° ring flips or 360° rotational diffusion often present. That is not the case however in the present compound with the solid remaining well ordered at least up to 323 K. In the nematic phase formed at 390 K, we may presume that increased intermolecular spacing relative to that in the solid allows the comparatively free rotation of the aromatic rings. Thus, there is expected to be a significant entropy change upon melting from the solid to nematic phase resulting from the onset of motion in previously static rings.

In summary, our experimental results using the DQ MAS technique indicate that the technique is likely to be a real alternative to selective deuteration in motional studies on complex materials and, furthermore, will allow complete motional studies on materials where selective deuteration is impossible.

ACKNOWLEDGMENT

The authors thank the Engineering and Physical Sciences Research Council of Great Britain for funding.

REFERENCES

1. H. W. Spiess, *Chem. Rev.* **91,** 1321 (1991).
2. A. K. Roy and P. T. Inglefield, *Prog. NMR Spectrosc.* **22,** 569 (1990).
3. T. M. Alam and G. P. Drobny, *Chem. Rev.* **91,** 1545 (1991).

4. D. Riechert, Z. Olender, R. Poupko, H. Zimmermann, and Z. Luz, *J. Chem. Phys.* **98,** 7699 (1993).
5. S. Vega, T. W. Shattuck, and A. Pines, *Phys. Rev. Lett.* **37,** 43 (1976).
6. S. Vega and A. Pines, *J. Chem. Phys.* **66,** 5624 (1977).
7. R. Eckman, L. Muller, and A. Pines, *Chem. Phys. Lett.* **74,** 376 (1980).
8. C. Chebli and F. Brisse, *Acta Crystallogr. C* **51,** 1164 (1995).
9. C. Schmidt, B. Blumich, and H. W. Spiess, *J. Magn. Reson.* **79,** 269 (1988).
10. R. R. Ernst, G. Bodenhausen, and A. Wokaun, ''Principles of Nuclear Magnetic Resonance in One and Two Dimensions,'' Chap. 1, Clarendon Press, Oxford (1987).
11. M. J. Duer and M. H. Levitt, *Solid State NMR* **1,** 211 (1992).
12. M. J. Duer and C. Stourton, *J. Magn. Reson.* **124,** 189 (1997).
13. A. Medek, J. S. Harwood, and L. Frydman, *J. Am. Chem. Soc.* **117,** 12779 (1995).
14. A. Abragam, ''Principles of Nuclear Magnetism,'' Chap. X, Clarendon Press, Oxford (1961).